



AIAA 2004-0364

**Toward Optimal Control of
Aeroacoustic Flows using
Discontinuous Galerkin
Discretizations**

Guoquan Chen
Rice University
Houston, TX 77005-1892

S. Scott Collis
Sandia National Laboratories
Albuquerque, NM 87185-1110

2004 AIAA Aerospace Sciences Meeting
January 5–8, 2004
Reno, NV

Toward Optimal Control of Aeroacoustic Flows using Discontinuous Galerkin Discretizations

Guoquan Chen*

Rice University

Houston, TX 77005-1892

S. Scott Collis†

Sandia National Laboratories ‡

Albuquerque, NM 87185-1110

Abstract

The coupling of accurate computational fluid dynamics analysis with optimal control theory has the potential to advance active flow-control for complex flows including flows involving aeroacoustic noise generation. However, achieving this requires computational tools with high accuracy and the flexibility to handle complex geometries with unstructured grids. To meet this goal, we present an optimal control framework for unsteady flows based on the Discontinuous Galerkin Method (DGM) and, in this paper, we apply this framework for both Burgers and compressible Navier–Stokes flows. DGM discretizations have several advantages for optimization studies including high formal accuracy, local *hp*-refinement, and the ability to handle unstructured grids. Both Burgers and Navier–Stokes optimal control problems are solved numerically using a DGM spectral-element discretization for spatial terms and fourth-order Runge–Kutta time integration and the control is updated using a nonlinear conjugate gradient method. The gradient computation is performed using a continuous adjoint-equation that is also discretized with DGM and fourth-order Runge–Kutta. Results for Burgers equations using both distributed and boundary control (Dirichlet and Neumann) are presented to validate our approach. We then present preliminary results for unsteady flows governed by the compressible Navier–Stokes equations including the suppression of vortex shedding in the wake of a circular cylinder. In the future, our DGM/optimal-control formulation will be used to develop active flow-control strategies for aeroacoustic applications and the paper ends with a preliminary state calculation for noise generation via blade-vortex-interaction.

Introduction

The numerical solution of optimal control problems governed by the unsteady compressible Navier–Stokes equations is a challenging problem that requires careful mathematical formulation, accurate state solution, efficient gradient computation, and convergent optimization algorithms. As a simplified model of the Navier–Stokes (NS) equation, the one-dimensional Burgers equation represents many of the properties of NS equations, such as nonlinear convection and viscous diffusion leading to shock waves and boundary layers. Given this, the viscous Burgers equation has received significant attention [1–3] and recent research has focused on the control of Burgers flow as a model for control of Navier–Stokes flows [2, 4]. To meet the challenges associated with optimal control of unsteady flow, we have developed a new computational framework based on the discontinuous Galerkin method (DGM) that allows for spectral accuracy on unstructured grids with the ability to use local *hp*-refinement. These capabilities will be of particular importance for large-scale optimal control for complex fluid flows such as those encountered in aeroacoustic applications. This paper presents our efforts in this direction by applying DGM to the solution of optimal control problems for flows governed by the viscous Burgers equation and preliminary results for the compressible Navier–Stokes equations.

Since the number of control variables is large in the problems that we target, an adjoint equation is utilized to efficiently evaluate the gradient of the objective functional with-respect-to the control. In general, there are two approaches to adjoint-based gradient evaluation: the optimize-then-discretize approach and discretize-then-optimize approach. One of the goals of our research is to evaluate and compare these two approaches for formulating and solving optimal control problems using DGM. In this paper, we focus on the optimize-then-discretize approach by presenting a discussion of the problem formulation, implementation, and results. While the focus of the current paper is for Burgers flows, some preliminary results for unsteady, compressible Navier–Stokes flows are provided at the end of the paper. A preliminary version of this paper was presented at the 2003 AIAA Region IV Student paper

*Ph.D. Candidate, Department of Mechanical Engineering and Materials Science, gqchen@rice.edu

†Senior Member of Technical Staff, Optimization and Uncertainty Estimation, sscoll@sandia.gov, member AIAA.

‡Sandia is a multiprogram laboratory operated by Sandia Corporation, a Lockheed Martin Company, for the United States Department of Energy under contract DE-AC04-94AL85000

Copyright © 2004 by the authors. Published by the American Institute of Aeronautics and Astronautics, Inc. with permission.

Problem Formulation

Governing equations

The Burgers equation is given by

$$\frac{\partial u}{\partial t} + \frac{1}{2} \frac{\partial u^2}{\partial x} - \nu \frac{\partial^2 u}{\partial x^2} = f + \Phi \quad (1)$$

with boundary conditions

$$\begin{aligned} u(0, t) &= \phi_L \\ u_{,x}(L, t) &= \phi_R \end{aligned} \quad (2)$$

and initial condition

$$u(x, 0) = u_0(x) \quad (3)$$

in which Φ is the distributed control, and ϕ_L and ϕ_R are the boundary controls, with the spatial domain $\Omega = [0, L]$. Here, we set the source term, $f = 0$.

Objective functional

For the Burgers control problems in this paper, the objective functional is defined as

$$\begin{aligned} \mathcal{J} &= \frac{\ell}{2} \int_{t_0}^{t_0+T} \int_0^L \Phi^2 dx dt + \frac{\ell_1}{2} \int_{t_0}^{t_0+T} \phi_L^2 dt \\ &+ \frac{\ell_2}{2} \int_{t_0}^{t_0+T} \phi_R^2 dt + \frac{\omega_1}{2} \int_{t_0}^{t_0+T} \int_0^L (u - \tilde{u})^2 dx dt \\ &+ \frac{\omega_2}{2} \int_0^L [u(x, t_f) - \bar{u}(x)]^2 dx. \end{aligned} \quad (4)$$

where \tilde{u} and \bar{u} are the distributed and terminal target states, respectively.

Optimality equations

First, we form a L^2 -inner product by introducing an adjoint variable λ as

$$\langle \mathcal{N}u, \lambda \rangle = \int_{t_0}^{t_0+T} \int_0^L \left(\frac{\partial u}{\partial t} + \frac{1}{2} \frac{\partial u^2}{\partial x} - \nu \frac{\partial^2 u}{\partial x^2} - \Phi \right) \lambda dx dt, \quad (5)$$

where $\mathcal{N}u = 0$ denotes the Burgers equation (1).

Computing the variation of (5) with respect to the state variable u , and integrating by parts yields

$$\begin{aligned} \langle u', \mathcal{N}^* \lambda \rangle &= \int_0^L u' \lambda \Big|_{t_f} dx + \int_{t_0}^{t_0+T} u \lambda u' \Big|_0^L dt \\ &- \int_{t_0}^{t_0+T} \nu \lambda \frac{\partial u'}{\partial x} \Big|_0^L dt + \int_{t_0}^{t_0+T} \nu \frac{\partial \lambda}{\partial x} u' \Big|_0^L dt \\ &- \int_{t_0}^{t_0+T} \int_0^L \lambda \Phi' dx dt, \end{aligned} \quad (6)$$

where \mathcal{N}^* denotes the adjoint operator, defined as

$$\mathcal{N}^* \lambda = -\frac{\partial \lambda}{\partial t} - u \frac{\partial \lambda}{\partial x} - \nu \frac{\partial^2 \lambda}{\partial x^2}. \quad (7)$$

The variation of the objective functional (4) with respect to the control is

$$\begin{aligned} \mathcal{J}' &= \ell \int_{t_0}^{t_0+T} \int_0^L \Phi \Phi' dx dt \\ &+ \ell_1 \int_{t_0}^{t_0+T} \phi_L \phi_L' dt + \ell_2 \int_{t_0}^{t_0+T} \phi_R \phi_R' dt \\ &+ \omega_1 \int_{t_0}^{t_0+T} \int_0^L (u - \tilde{u}) u' dx dt \\ &+ \omega_2 \int_0^L (u_{t_f} - \bar{u}) u_{t_f}' dx. \end{aligned} \quad (8)$$

According to the theory of Lagrange multipliers,

$$\mathcal{J}' - \langle \mathcal{N}u, \lambda \rangle' = 0$$

gives the adjoint equation

$$-\frac{\partial \lambda}{\partial t} - u \frac{\partial \lambda}{\partial x} - \nu \frac{\partial^2 \lambda}{\partial x^2} = \omega_1 (u - \tilde{u}) \quad (9)$$

with the boundary conditions

$$\begin{aligned} \lambda(0, t) &= 0 \\ u \lambda(L, t) + \nu \lambda_{,x}(L, t) &= 0 \end{aligned} \quad (10)$$

and end condition

$$\lambda(x, t_f) = \omega_2 (u(x, t_f) - \bar{u}(x)). \quad (11)$$

The optimality conditions are the state-equation (1) with boundary conditions (2) and initial condition (3), the adjoint equation (9) with boundary conditions (10) and end condition (11) and the gradient equations, given by

$$\begin{aligned} \nabla_{\Phi} \mathcal{J} &= \ell \Phi + \lambda, \\ \nabla_{\phi_L} \mathcal{J} &= \ell_1 \phi_L + \nu \frac{\partial \lambda}{\partial x} \Big|_{x=0}, \\ \nabla_{\phi_R} \mathcal{J} &= \ell_2 \phi_R + \nu \lambda_{x=L}. \end{aligned}$$

Solution of the optimality equations yields the gradient of the objective functional with respect to the control which should be equal to zero at the optimum. We use a nonlinear conjugate gradient method to solve this optimization problem and more details regarding optimal control of Burgers flows can be found in [5].

Numerical Method

The optimality equations are discretized with a discontinuous Galerkin method in space and fourth-order accurate Runge-Kutta time-integration.

Spatial Discretization

We denote the boundary of the domain Ω as $\partial\Omega = \Gamma_D \cup \Gamma_N$ where Γ_D is the portion of the boundary where Dirichlet conditions are specified and Γ_N is the portion of the boundary where Neumann conditions are set. The spatial domain Ω is partitioned into a set of non-overlapping

elements Ω_e that each have a Lipschitz boundary $\partial\Omega_e$. The element boundary is denoted as $\Gamma = \{\Gamma_D, \Gamma_N, \Gamma_0\}$ where Γ_0 are the inter-element boundaries. Let Ω_1 and Ω_2 be two adjacent elements; let $\Gamma_{12} = \partial\Omega_1 \cap \partial\Omega_2$; and let $\mathbf{n}^{(1)}$ and $\mathbf{n}^{(2)}$ be the corresponding outward unit normal vectors at that point.

Let $u^{(e)}$ and $F^{(e)}$ be the trace of a state u and flux vector F , respectively, on Γ_{12} from the interior of sub-domain Ω_e . Then, we define the average $\langle \cdot \rangle$ and jump $[\cdot]$ operators on Γ_{12} as

$$[u] = u^{(1)}\mathbf{n}^{(1)} + u^{(2)}\mathbf{n}^{(2)} \quad (12a)$$

$$[F_n] = F^{(1)}\mathbf{n}^{(1)} + F^{(2)}\mathbf{n}^{(2)}, \quad (12b)$$

$$\langle u \rangle = \frac{1}{2} (u^{(1)} + u^{(2)}), \quad (12c)$$

$$\langle F \rangle = \frac{1}{2} (F^{(1)} + F^{(2)}), \quad (12d)$$

where $F_n = F\mathbf{n}$ and $n = -1$ on a left boundary and $n = 1$ on a right boundary. Defining the convective and viscous fluxes as

$$F = \frac{u^2}{2}, \quad F^v = \nu u_{,x},$$

the discontinuous Galerkin formulation for the Burgers equation is

$$\begin{aligned} & \sum_e \int_{\Omega_e} \left\{ w(u_{,t} - \Phi) + w_{,x}(F^v - F) \right\} d\Omega - \\ & \int_{\Gamma_0} [wn] \langle \hat{F}^v - F \rangle d\Gamma - \int_{\Gamma_0} \langle \nu w_{,x} \rangle [n(\hat{u} - u)] d\Gamma \\ & - \int_{\Gamma_D} (\nu w_{,n})(u - \phi_L) + w \left(F_n^v - \hat{F}_n^v(u, \phi_L) \right) d\Gamma \\ & - \int_{\Gamma_N} w(\nu \phi_R - \hat{F}_n^v(u, u)) d\Gamma = 0 \quad (13) \end{aligned}$$

where \hat{F} , \hat{F}^v and \hat{u} are numerical fluxes. For the convective numerical inviscid flux, we use the Lax-Friedrichs flux [6], which can be expressed as

$$\hat{F}(u^-, u^+) = \frac{1}{2} [F(u^-) + F(u^+) + \lambda_m(u^- - u^+)]$$

where $\lambda_m = |\partial F / \partial u|$. For the numerical viscous flux, \hat{F}^v , and solution flux, \hat{u} , we use the Bassi-Rebay method [7, 8]. All boundary conditions are enforced weakly through the numerical fluxes and additional details regarding weak boundary condition enforcement can be found in [9, 10]

The DGM discretization for the adjoint equation (9) is similar to that of state (13),

$$\begin{aligned} & \sum_e \int_{\Omega_e} \left\{ w(\lambda_{,t} - \lambda u_{,x} + \omega_1(u - \tilde{u})) - \right. \\ & \quad \left. w_{,x}(G^v + G) \right\} d\Omega + \\ & \int_{\Gamma_0} [wn] \langle \hat{G}^v + G \rangle d\Gamma + \int_{\Gamma_0} \langle \nu w_{,x} \rangle [n(\hat{\lambda} - \lambda)] d\Gamma \\ & - \int_{\Gamma_D} \left\{ \nu w_{,n}\lambda - w \left(G_n^v - \hat{G}_n^v(\lambda, 0) \right) \right\} d\Gamma \\ & + \int_{\Gamma_N} w(-u\lambda - \hat{G}_n^v(\lambda, \lambda)) d\Gamma = 0 \quad (14) \end{aligned}$$

where $G \equiv u\lambda$ and $G^v \equiv \nu\lambda_{,x}$. Similar to the state discretization, we use the Lax-Friedrichs and Bassi-Rebay numerical fluxes and the adjoint boundary conditions (10) are applied in evaluating the numerical fluxes on the domain boundary.

Temporal Discretization

A fourth-order accurate explicit Runge-Kutta method is used, which is symmetric and therefore well-suited for optimal control problems [11].

Results

The following results all use the continuous adjoint approach presented above. For all cases, the initial condition is the same as that in Chang's Ph.D. thesis [5] and is given by

$$u_0(x) = \sin(m\pi \tan(c_s(2x - 1)) / \tan(c_s)) \quad (15)$$

where c_s is a parameter that controls the stretching of the initial profile. This initial profile can lead to boundary layers near the domain ends. We choose $c_s = 1.3$. Our space and time domain are $0 \leq x \leq 1$ and $0 \leq t \leq 1$, respectively. The viscosity for all cases is $\nu = 0.01$. For spatial discretization, the domain is divided into 40 equally sized elements. Unless otherwise specified, fourth-order ($p = 4$) polynomial representations are used on each element and the time-step is $\Delta t = 0.00025$.

Distributed Control

The first test case corresponds to that done in Ref. [5] and is used to validate our implementation. The control objective is to sustain the initial profile, so the objective functional is defined as

$$\begin{aligned} \mathcal{J} &= \frac{\ell}{2} \int_0^1 \int_0^1 \Phi^2 dx dt \\ &+ \frac{1}{2} \omega_1 \int_0^1 \int_0^1 (u - u_0)^2 dx dt \\ &+ \frac{1}{2} \omega_2 \int_0^1 [u(x, 1) - u_0]^2 dx. \quad (16) \end{aligned}$$

In our simulations, $\omega_1 = 1$, $\omega_2 = 1$, and $\ell = 0.01$.

Figure 1 shows that as the number of optimization iterations increases, the state solution at $t = t_f = 1$ becomes closer and closer to the target solution. The distributed optimal control profile, $\Phi(x)$, is shown in Fig. 2 after four optimization iterations which demonstrates that the control has boundary layers near the left and right boundaries and that the control changes in time in order to drive the solution toward the target state.

The evolution of the objective function, J , as the number of optimization iterations increases is shown in Fig. 3. From this figure, we see that the objective functional drops to a value of 8×10^{-3} with no significant decrease in J beyond about 3 iterations which is consistent with prior results [5]. Taking advantage of the ability to perform p -refinement in DGM, Fig. 3 also shows results for both

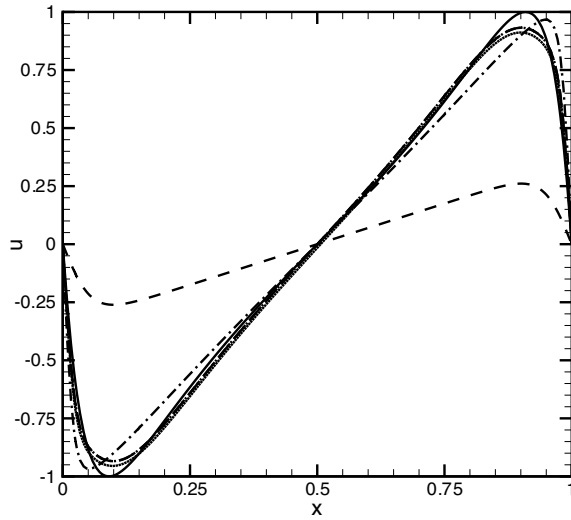


Fig. 1 Distributed control of Burgers equation for $p = 4$: — initial profile; ---- the profile without control at $t = 1$; -.- profile with control at $t = 1$ after first iteration; --- profile with control at $t = 1$ after second iteration; profile with control $t = 1$ after third iteration.

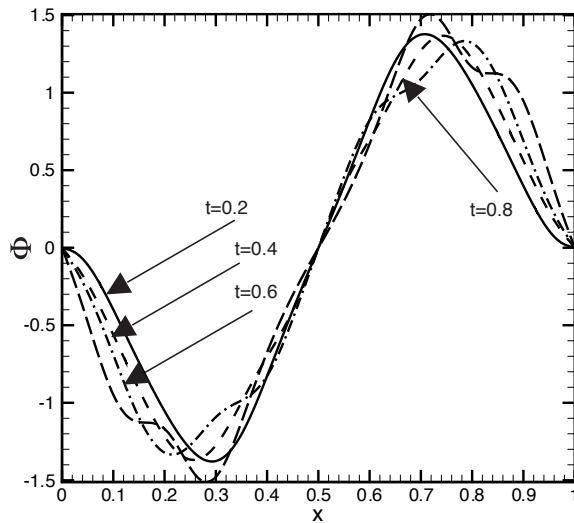


Fig. 2 Distributed control profile after fourth iteration at $t = 0.2, 0.4, 0.6$, and 0.8 .

$p = 2$ and $p = 6$. Overall the optimal-control solutions are similar for all values of p which indicates that this distributed control problem is well resolved, even at $p = 2$.

Boundary Control

In order to validate our implementation for boundary control, we formulate our test cases as inverse problems. Given a specified boundary condition, the corresponding state solutions are first obtained, which then become our objective solution \tilde{u} . Using this as our objective solution in the objective functional, we then solve the optimal control problem and compare the computed boundary values to the boundary condition that was originally prescribed.

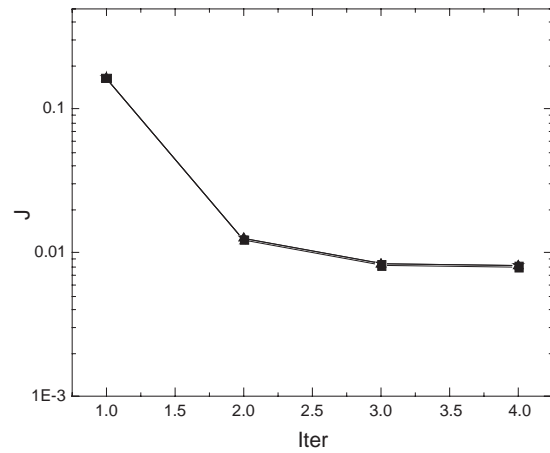


Fig. 3 Objective functional, J , at different iterations for distributed control: ■ $p = 2$; △ $p = 4$; ◇ $p = 6$.

Dirichlet Boundary Control

The initial condition is the same as that used for distributed control. Our control objective is to achieve the objective solution \tilde{u} , which is obtained using the prescribed boundary condition $\phi_L^* = 2t^2$. Thus, the objective functional is

$$\begin{aligned} \mathcal{J} = & \frac{\ell_1}{2} \int_0^1 \phi_L^2 dt \\ & + \frac{\omega_1}{2} \int_0^1 \int_0^1 (u - \tilde{u})^2 dx dt \\ & + \frac{1}{2} \omega_2 \int_0^1 [u(x, t_f) - \tilde{u}(x, t_f)]^2 dx \end{aligned} \quad (17)$$

where $\omega_1 = 1000$, $\omega_2 = 1$, and $\ell_1 = 0.001$. The initial guess for the boundary control is $\phi_L = 2t_f t$ so that the final boundary condition is satisfied at $t = 0$.

Comparing the target state and the optimal state solutions after 24 iterations (see Fig. 5) shows that the agreement is excellent. It is also shown in Fig. 6 that the control converges to the target boundary condition $\phi_L^* = 2t^2$. This can be seen more clearly in Fig. 7 which shows the error in the computed control compared to the target boundary condition.

Figure 8 presents the evolution of the objective functional showing that the value converges after about 20 optimization iterations for $p = 4$. Also shown in Fig. 8 are convergence histories for other values of p . Improving resolution does appear to lead to a slightly smaller value of J although convergence is slightly slower for larger p .

Neumann Boundary Control

We now consider Neumann boundary control where the control variable is ϕ_R at $x = 1$. Our control objective is to sustain the target solution \tilde{u} obtained using the prescribed boundary condition $\phi_R^* = -31.52(1 - 2\sqrt{t})$. The objective

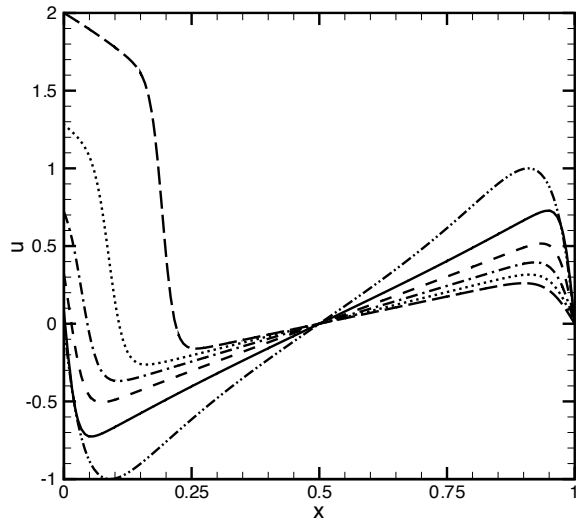


Fig. 4 State solution with prescribed Dirichlet boundary condition $\phi_L^* = 2t^2$ for $p = 4$: \cdots initial profile; — the profile at $t = 0.2$; --- profile at $t = 0.4$; $\text{-}\cdot\text{---}$ profile at $t = 0.6$; \cdots profile at $t = 0.8$; --- profile at $t = 1$.

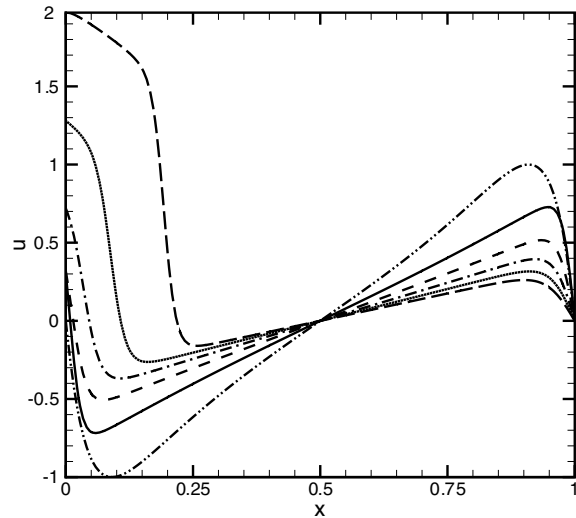


Fig. 5 Final optimal state solution using Dirichlet boundary control for $p = 4$: \cdots initial profile; — the profile at $t = 0.2$; --- profile at $t = 0.4$; $\text{-}\cdot\text{---}$ profile at $t = 0.6$; \cdots profile at $t = 0.8$; --- profile at $t = 1$.

functional for this problem is defined as

$$\begin{aligned} \mathcal{J} = & \frac{\ell_2}{2} \int_0^1 \phi_R^2 dt \\ & + \frac{\omega_1}{2} \int_0^1 \int_0^1 (u - \tilde{u})^2 dx dt \\ & + \frac{1}{2} \omega_2 \int_0^1 [u(x, t_f) - \tilde{u}(x, t_f)]^2 dx \end{aligned} \quad (18)$$

where $\omega_1 = 100,000$, $\omega_2 = 1$, and $\ell_2 = 1 \times 10^{-7}$. The initial control is the linear distribution $\phi_R = -31.52(1 - 2\sqrt{t_f})t/t_f$.

After several iterations, the optimal solution becomes almost identical to the target solution as seen by comparing

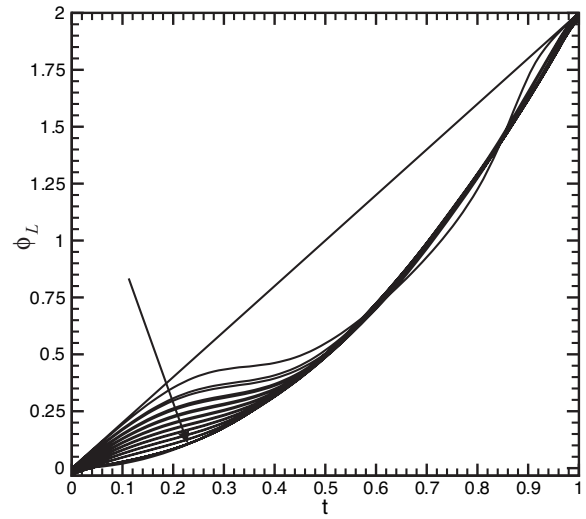


Fig. 6 Iteration history for Dirichlet optimal control with $p = 4$. The arrow shows the direction of increasing optimization iterations.

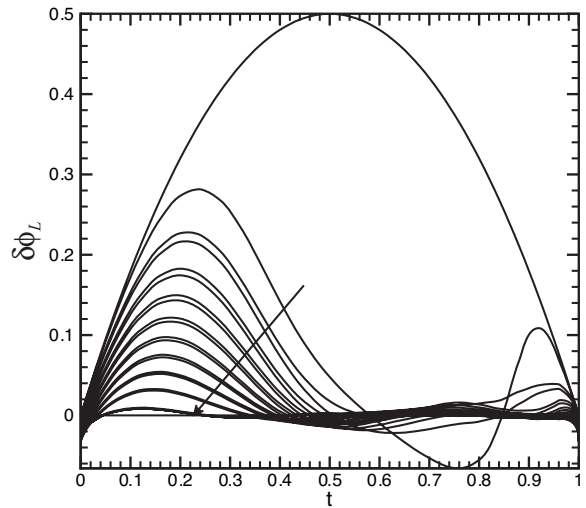


Fig. 7 Iteration history for the error in the Dirichlet optimal control with $p = 4$. The arrow shows the direction of increasing optimization iterations.

the target solution (Fig. 9) with the final optimal state solution after 24 optimization iterations (Fig. 10).

Good convergence is also obtained in the control profiles (Fig. 11), however, by plotting the difference between the optimal control and the target control (Fig. 12) we see that even after 24 iterations there are noticeable differences between the two, especially for early times. These differences are larger than those encountered for Dirichlet control. Figure 13 shows the convergence history for the objective function, J , for both $p = 4$ as well as other values of p . Increases in p beyond a value of 4 do not lead to a significant change in the optimal solution. It is important to remember that a gradient-based optimization algorithm only finds local minima — there is no guarantee that the global minima will be found. Thus it is possible that the current results are at a local optimum which would explain why we are not able to exactly recover the prescribed con-

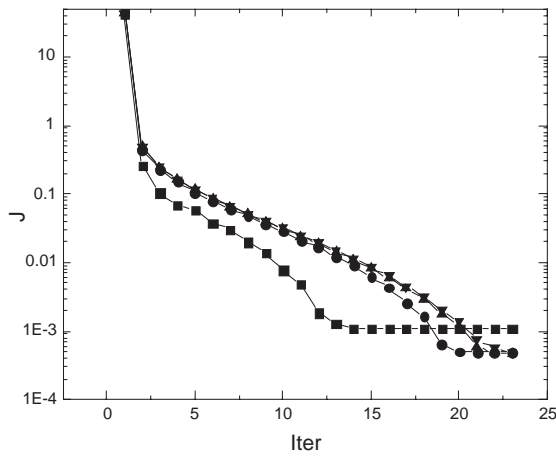


Fig. 8 Evolution of the objective functional, J , for Dirichlet control, \blacksquare $p = 2$; \bullet $p = 4$; \triangle $p = 6$; ∇ $p = 7$.

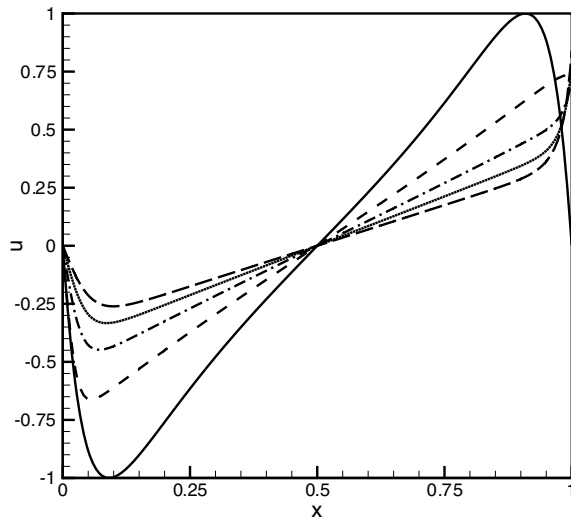


Fig. 9 State solution with prescribed Neumann boundary condition $\phi_R^* = -31.52(1 - 2\sqrt{t})$ using $p = 4$: — initial profile; ---- the profile at $t = 0.25$; —·— profile at $t = 0.5$; profile at $t = 0.75$; --- profile at $t = 1$.

trol profile for this inverse problem.

To determine whether an improved optimal solution can be obtained for this problem, we considered two additional initial guesses for the control profile. First, we added very small perturbations to the target control profile so that the initial control profile took the form $\phi_R = -31.52(1 - 2\sqrt{t}) + \varepsilon$. In this case the optimal control quickly converged to the target control. Next, we tried an initial control that contained a finite-amplitude oscillation about the target control, i.e. $\phi_R = -31.52(1 - 2\sqrt{t}) + 30t(1 - t)$. With this starting profile, Figs. 14 and 15 show that after several iterations, the optimal control almost recovers the target control profile. This is also seen in Fig. 16 which compares the evolution of J given two different initial control distributions. Clearly, these two cases lead to a more optimal solution confirming the fact that the first case was a local minimum.

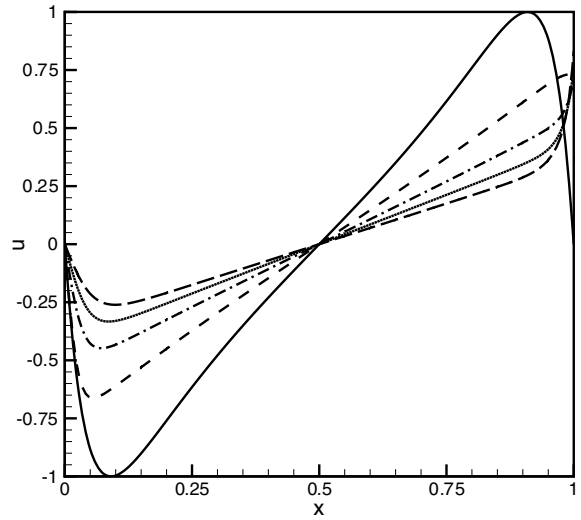


Fig. 10 Final optimal state solution for Neumann boundary control using $p = 4$: — initial profile; ---- the profile at $t = 0.25$; —·— profile at $t = 0.5$; profile at $t = 0.75$; --- profile at $t = 1$.

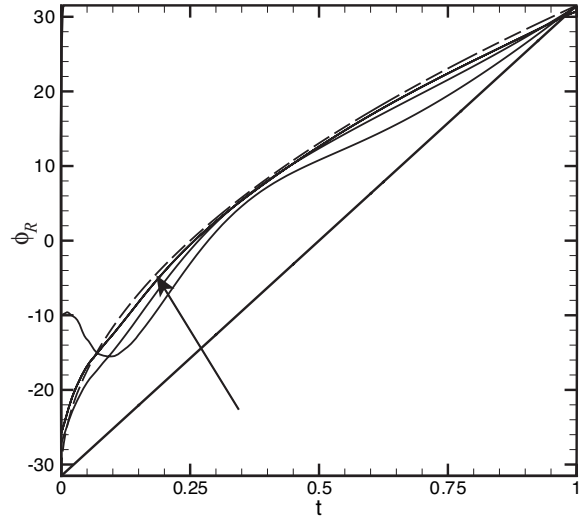


Fig. 11 Iteration history for Neumann optimal control using $p = 4$. The arrow shows the direction of increasing optimization iterations.

Summary of Burgers Control

In the prior sections we have described our continuous adjoint formulation and implementation for optimal control of problems governed by the unsteady Burgers equation where both the state and adjoint equations are discretized using discontinuous Galerkin in space. Results were presented for distributed control as well as both Dirichlet and Neumann boundary control and, in all cases, reductions in the objective function of at least one order of magnitude (or more) were obtained with a modest number (less than 6) of optimization iterations. Similar reductions in the gradient of the objective function (not shown here, but see Fig. 20 for similar results for Navier–Stokes flows) are also obtained indicating that our solutions are indeed approaching optimality. These results for Burgers control give us con-

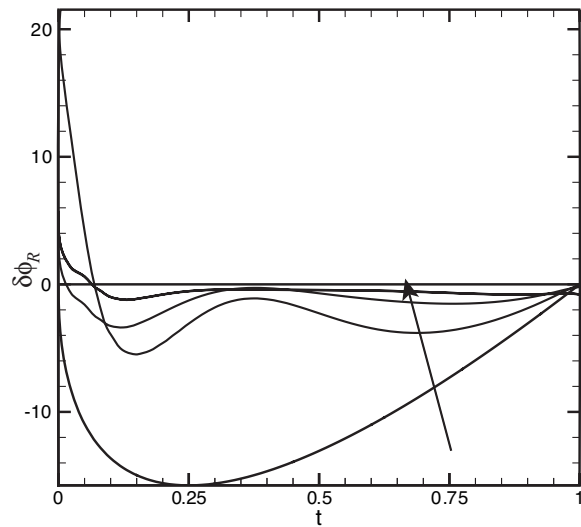


Fig. 12 Iteration history for the error in the Neumann optimal control for $p = 4$. The arrow shows the direction of increasing optimization iterations.

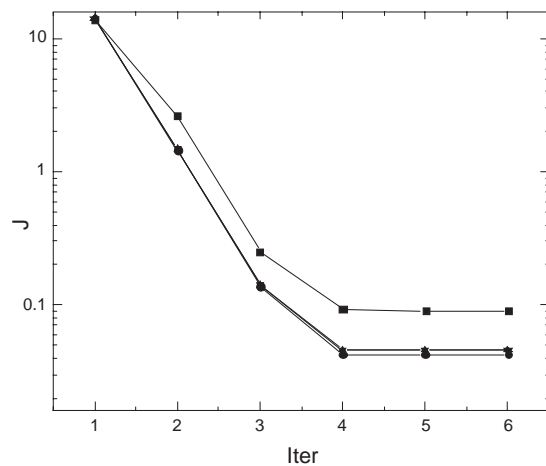


Fig. 13 Evolution of the objective functional, J , for optimal Neumann boundary control: \blacksquare $p = 2$; \bullet $p = 4$; \triangle $p = 6$; ∇ $p = 7$.

fidence in both our formulation and implementation of the continuous adjoint equation, boundary conditions, and gradient evaluation. With this, we now present some preliminary results for optimal control of unsteady Navier–Stokes flows.

Optimal Control of Cylinder Wakes

We are currently working to extend our capability to include optimal boundary control of unsteady, compressible Euler and Navier–Stokes flows. In order to validate our approach, we consider the control of the unsteady wake behind a circular cylinder at low Reynolds numbers. Considerable research has been conducted for cylinder wake control using a variety of approaches including distributed controls, boundary control, and cylinder rotation (see e.g., Refs. [12–16]).

We consider steady suction/blowing on the entire cylin-

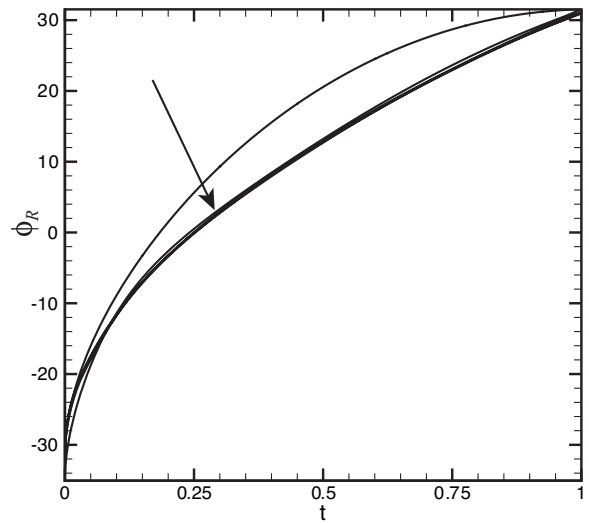


Fig. 14 Iteration history for Neumann boundary control starting from initial control $\phi_R = -31.52(1 - 2\sqrt{t}) + 30t(1 - t)$ and using $p = 6$. The arrow shows the direction of increasing optimization iterations.

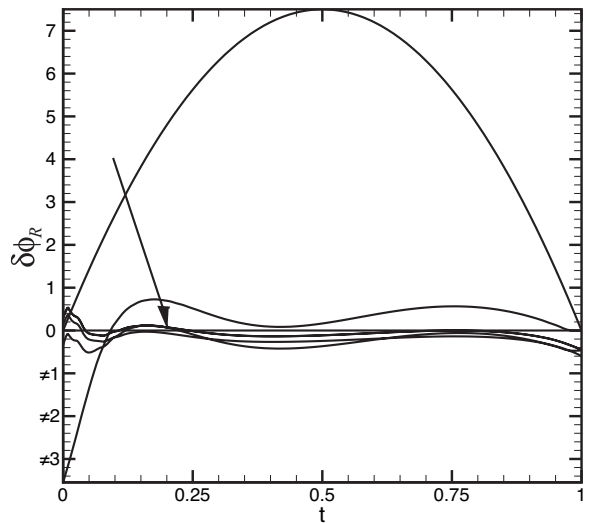


Fig. 15 Iteration history for the error in the Neumann boundary control starting from initial control $\phi_R = -31.52(1 - 2\sqrt{t}) + 30t(1 - t)$ and using $p = 6$. The arrow shows the direction of increasing optimization iterations.

der surface as the control and find an optimal spatial distribution of the control to drive the unsteady wake at $Re = 100$ to match the steady wake at $Re = 20$, both at a freestream Mach number of 0.3. Our problem setup is similar to that of Li *et al.* [16], although we consider compressible flow with somewhat different boundary conditions, a slightly modified objective function (described below), and our control is distributed over the entire cylinder surface. The domain (see Fig. 17) is rectangular $\Omega = [-3, 19] \times [-3, 3.1]$ with the cylinder center located at $(0, 0)$. A block structured mesh using 576 quadrilaterals was generated using a special purpose grid generator [17] and each quadrilateral has polynomial order $p = 4$.

While the problem geometry described above is the same

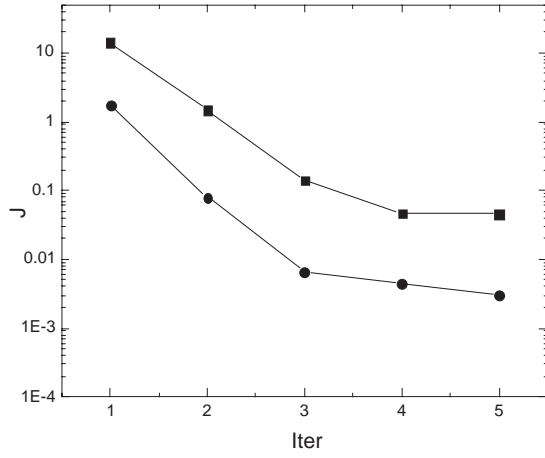


Fig. 16 Comparison of objective functionals J for Neumann control with different initial control profiles using $p = 6$: ▲ initial control profile $\phi_R = -31.52(1 - 2\sqrt{t_f}t/t_f)$; ● initial control profile $\phi_R = -31.52(1 - 2\sqrt{t}) + 30t(t_f - t)$.

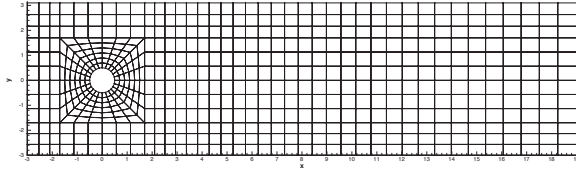


Fig. 17 Element mesh for cylinder wake control.

as in Ref. [16], we use non-reflecting boundary conditions on the top and bottom boundaries, while slip walls were imposed in [16]. Since our formulation is compressible, we must also prescribe a thermal boundary condition at the cylinder surface and the results presented here use an adiabatic wall boundary condition. Additional details regarding the problem setup, discretization, and state solutions can be found in [9].

Objective functionals

Similar to that in [16], the objective functional for the current problem is defined as a full flowfield tracking problem where the controlled flow is driven toward the steady laminar flow at $Re = 20$. Thus, our objective is to control the unsteady flow at $Re = 100$ so that it approaches the steady flow at $Re = 20$ and we define our objective function as

$$\begin{aligned} \mathcal{J} = & \frac{1}{2} \int_t \int_{\Omega} ((\rho - \rho_o)^2 + (\rho u - \rho_o u_o)^2 \\ & + (\rho v - \rho_o v_o)^2 + (\rho E - \rho_o E_o)^2) d\Omega dt \\ & + \frac{\omega_1}{2} \int_t \int_{\Gamma_c} g^2 d\Gamma dt \end{aligned} \quad (19)$$

where $\rho_o, \rho_o u_o, \rho_o v_o, \rho_o E_o$ are the conservation variables of the target flow field (steady flow at $Re = 20$) and g is the steady control (blowing/suction velocity) on the cylinder surface, Γ_c . Due to our compressible formulation, our objective function targets differences in the conservation variables while Li *et al.* target differences in the velocity

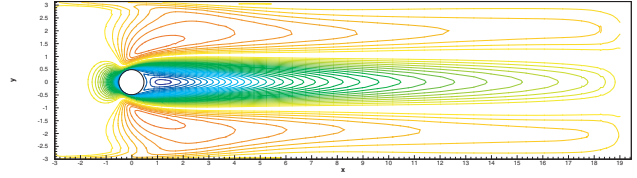


Fig. 18 Contours of streamwise momentum, ρu , for the uncontrolled steady-state solution at $Re = 20$.

components. In the future, we will also consider a velocity tracking objective functional. Similar to Li *et al.* [16] we define our time window, T , as one shedding period. After obtaining an adequately converged optimal control distribution, we then continue advancing the solution using this steady control profile to observe its long time influence on the flow.

Adjoint formulation

The gradient computation is based on the continuous adjoint formulation for the Navier–Stokes equations described in [18–21] and these adjoint equations are discretized using DGM. Details of the formulation and implementation will appear in forthcoming publications. Similar to the Burgers problems described above, the adjoint solution is used to compute the gradient of the objective functional with respect to the control and a nonlinear conjugate gradient method is used to update the control. Details will appear in subsequent publications.

Results

Figure 18 presents streamwise momentum contours for the steady laminar flow state at $Re = 20$, which is our target solution. Figure 19 shows snapshots of the uncontrolled flow at $Re = 100$ during one vortex shedding period which takes the form typical of the Kármán vortex street.

Starting from the fully developed Kármán vortex street at $Re = 100$, we then proceed to solve the optimal control problem described above and the convergence history of the objective functional and norm of the gradient of the objective function are shown in Fig. 20. The majority of the reduction in J occurs in the first 4 iterations which is similar to observed for the Burgers control problems discussed above. However, gradient of the objective function continues to decrease with additional iterations and drops by more than two orders of magnitude after 20 iterations (recall that it is the square of the gradient norm that is plotted in Fig. 20.)

Taking the control distribution after 20 iterations as the optimal solution, we then continued the simulation for an additional 20 vortex shedding periods and snapshots of streamwise momentum are shown in Fig. 21. Clearly, the vortex shedding is nearly suppressed by $t = 40$ (and computations for longer times verifies that shedding is completely suppressed). These results are qualitatively similar to the incompressible results of Li *et al.* [16] and our future work will report in greater detail issues in optimal control of circular cylinder wakes for compressible flows. Likewise, given this success, we will also apply our control

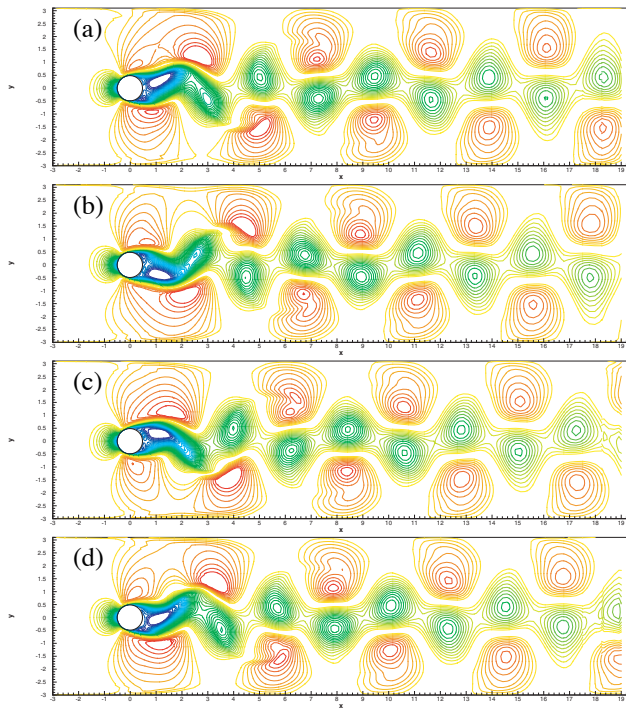


Fig. 19 Contours of streamwise momentum, ρu , for one vortex shedding period for the uncontrolled flow at $Re = 100$: (a) $t = 0.2$, (b) $t = 0.8$, (c) $t = 1.4$, and (d) $t = 2$.

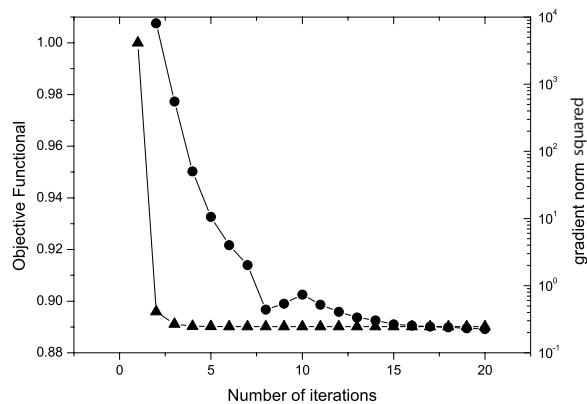


Fig. 20 Optimization history for the objective functional and the norm of the gradient of the objective functional squared. The optimization time window is one shedding period which corresponds to 2 time units: • gradient norm squared; ▲ objective functional.

framework for optimal control of aeroacoustic flows and preliminary steps in this direction are described in the next section.

Progress Toward Aeroacoustic Control

A practical problem of interest for aeroacoustic flow control is suppression of the noise arising from Blade Vortex Interaction (BVI) that can occur for rotor-craft in low speed, descending flight conditions. While there have been a number of different and widely varied approaches to controlling BVI noise presented in the literature (see [19] and reference therein for a brief review), our research group has been interested in developing on-blade controls using

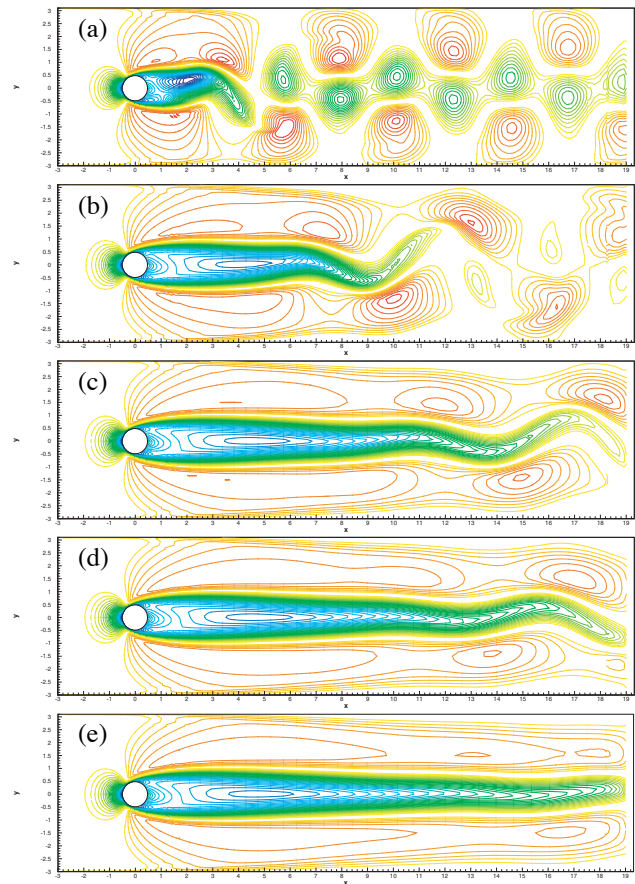


Fig. 21 Contours of streamwise momentum, ρu , for the controlled flow at $Re = 100$: (a) $t = 2$, (b) $t = 14$, (c) $t = 26$, (d) $t = 30$, (e) $t = 40$. Note that the steady optimal control is obtained over the first two time units, but is then used throughout the remainder of the computation.

optimal control theory. In the recent work of Collis *et al.* [19], it is shown for a model BVI problem that a 13db reduction in forward scattered sound can be achieved with small amplitude suction/blowing near the leading edge. Unfortunately, the computational tools developed and used in [19] are not able to represent the complex geometries and flows encountered in more realistic problems. This, in fact, was the motivation to develop the current DGM based tool described here.

As an example of the potential of our current DGM based approach, Fig. 22 shows contours of pressure from the parallel interaction of a vortex with a Bell AH-1 rotor blade. Exploiting the local conservation property of DGM, this simulation uses a novel multi-model approach with the Navier–Stokes equations solved near the blade surface and in the wake, the linear Euler equations in the farfield, and a sponge (or buffer) region used to absorb unsteady vortical motions near the outflow boundary. This multi-model approach can lead to significant improvements in computations efficiency with little or no loss of fidelity. Future publications will describe this multi-model formulation in detail and we are currently extending our optimal control framework for these types of challenging aeroacoustic control problems.

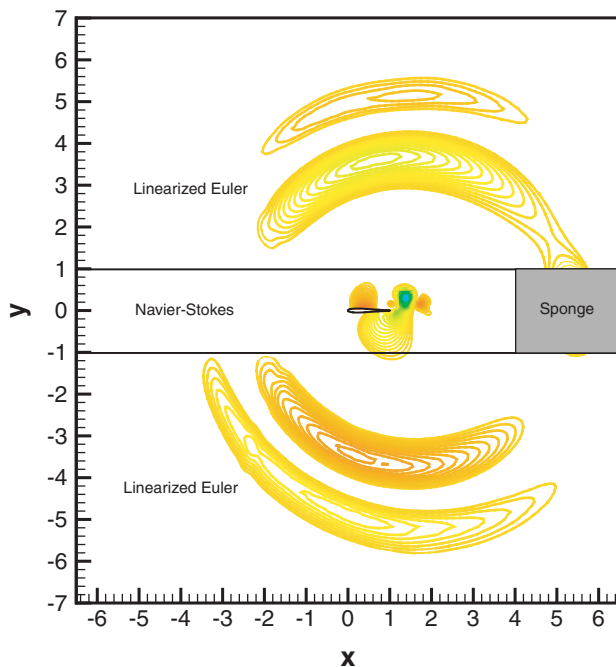


Fig. 22 Contours of scattered pressure, p , for a single vortex interacting with a Bell AH-1 rotor blade.

Conclusions and Future Work

This work focuses on the application of discontinuous Galerkin methods for optimal control of unsteady flows. We have derived the optimality system, including the continuous adjoint equation for viscous Burgers and compressible Navier–Stokes state equations. Both state and adjoint equations are discretized using the discontinuous Galerkin method. Optimal control results are presented for distributed and boundary control of Burgers flows and these results validate our formulation and implementation. Preliminary results for boundary control of compressible Navier–Stokes flows are presented for suppression of unsteady shedding from a circular cylinder. By optimizing over only one shedding period, we obtain a steady distribution of surface normal velocity that suppresses shedding at $Re = 100$ and our results are in qualitative agreement with recently reported incompressible results. Both the Burgers and Navier–Stokes studies demonstrate good performance for our continuous adjoint formulation and DGM discretization. A novel feature of DGM is that all boundary conditions are set weakly through numerical fluxes and these results demonstrate the viability of this method for boundary control. Our future work will apply a similar formulation for optimal control of multidimensional Navier–Stokes flows with application to aeroacoustic flow control.

Acknowledgments

This work is partially supported by Texas ATP grant 003604-0011-2001, NSF grant 0116289-2001, and the Department of Energy. The authors have benefited from helpful discussions with Dr. Kaveh Ghayour and Dr. Matthias Heinkenschloss, both of Rice University.

References

- ¹Chambers, D. H., Adrian, R. J., Moin, P., and Stewart, D. S., “Karhunen–Loève Expansions of Burgers’ model of Turbulence,” *Phys. Fluids*, Vol. 10, 1988, pp. 2573–2582.
- ²Choi, H., Temam, T., Moin, P., and Kim, J., “Feedback control for unsteady flow and its application to the stochastic Burgers equation,” *J. Fluid Mech.*, Vol. 253, 1993, pp. 509–543.
- ³Kunisch, K. and Volkwein, S., “Control of Burger’s equation by a reduced order approach using proper orthogonal decomposition,” *J. Opt. Th. App.*, Vol. 102, No. 2, 1999, pp. 345–371.
- ⁴Berggren, M., Glowinski, R., and Lions, J. L., “A Computational Approach to Controllability Issues for Flow-Related Models. (I): Pointwise Control of the Viscous Burgers equation,” *International Journal for Numerical Methods in Fluids*, Vol. 7, 1996, pp. 237–252.
- ⁵Chang, Y., *Reduced Order Methods for Optimal Control of Turbulence*, Ph.D. thesis, Rice University, Mechanical Engineering and Materials Science, 2000.
- ⁶Cockburn, B., editor, *High-order methods for computational applications, Lecture Notes in Computational Science and Engineering*, chap. Discontinuous Galerkin methods for convection-dominated problems, Springer, Berlin, 1999, pp. 69–224.
- ⁷Bassi, F. and Rebay, S., “A High-Order Accurate Discontinuous Finite Element Method for the Numerical Solution of the Compressible Navier–Stokes Equations,” *J. Comp. Phys.*, Vol. 131, 1997, pp. 267–279.
- ⁸Bassi, F. and Rebay, S., “A High Order Discontinuous Galerkin Method for Compressible Turbulent Flows,” *Discontinuous Galerkin Methods: Theory, Computation, and Applications*, edited by B. Cockburn, G. E. Karniadakis, and C.-W. Shu, No. 11 in Lecture Notes in Computational Science and Engineering, Springer, 2000, pp. 77–88.
- ⁹Collis, S. S. and Ghayour, K., “Discontinuous Galerkin for Compressible DNS,” *ASME paper number FEDSM2003-45632*, 2003.
- ¹⁰Collis, S. S., “Discontinuous Galerkin Methods for Turbulence Simulation,” *Proceedings of the 2002 Center for Turbulence Research Summer Program*, 2002, pp. 155–167.
- ¹¹Hager, W. W., “Runge–Kutta Methods in Optimal Control and Transformed Adjoint System,” *Numerische Mathematik*, Vol. 87, No. 2, 2000, pp. 247–282.
- ¹²Park, D., Ladd, D., and Hendricks, E., “Feedback control of Karman vortex shedding,” 1992.
- ¹³Sritharan, S., Ou, Y., Park, D., and Ladd, D., “Optimal control of viscous flow past a cylinder: mathematical theory, computation and experiment-Part I. Actual Problems of Aviation and Aerospace Systems,” *Russ-Am Sci J*, Vol. 1, 1996, pp. 5–15.
- ¹⁴Sritharan, S., Ou, Y., Park, D., and Ladd, D., “Optimal control of viscous flow past a cylinder: mathematical theory, computation and experiment-Part II. Actual Problems of Aviation and Aerospace Systems,” *Russ-Am Sci J*, Vol. 2, 1996, pp. 7–18.
- ¹⁵Homescu, C., Navon, I. M., and Li, Z., “Suppression of Vortex Shedding for Flow Around a Circular Cylinder Using Optimal Control,” *International Journal for Numerical Methods in Fluids*, Vol. Volume 38, Issue 1, 2002, pp. 43–69.
- ¹⁶Zhijin Li, I. Michael Navon, M. H. and Dimet, F. L., “Optimal Control of Cylinder Wakes via Suction and Blowing,” *Computers & Fluids*, Vol. Volume 32, Issue 2, 2003, pp. 149–171.
- ¹⁷Tezduyar, T. E., “Stabilized Finite Element Formulations for Incompressible Flow Computations,” *Adv. Appl. Mech.*, Vol. 28, 1991, pp. 1–44.
- ¹⁸Collis, S. S., Ghayour, K., Heinkenschloss, M., Ulbrich, M., and Ulbrich, S., “Numerical Solution of Optimal Control Problems Governed by the Compressible Navier–Stokes Equations,” *International Series of Numerical Mathematics*, Vol. 139, Birkhäuser Verlag, 2001, pp. 43–55.
- ¹⁹Collis, S. S., Ghayour, K., and Heinkenschloss, M., “Optimal Control of Aeroacoustic Noise Generated by Cylinder Vortex Interaction,” *Int. J. Aero.*, Vol. 1, No. 2, 2002, pp. 97–114.
- ²⁰Collis, S. S., Ghayour, K., and Heinkenschloss, M., “Optimal Control of Aeroacoustics: Transpiration Boundary Control,” *AIAA J.*, Vol. 41, No. 7, July 2003.
- ²¹Chen, G. and Collis, S. S., “Optimal control of viscous flow using the discontinuous Galerkin method,” draft.